ACS Biomaterials SCIENCE & ENGINEERING

pubs.acs.org/journal/abseba

Article

One-Pot Assembly of Drug-Eluting Silk Coatings with Applications for Nerve Regeneration

Tanner D. Fink, Jessica L. Funnell, Ryan J. Gilbert, and R. Helen Zha*

Cite This: *ACS Biomater. Sci. Eng.* 2024, 10, 482−496

Read Online

ACCESS | Metrics & More | Article Recommendations | Supporting Information

ABSTRACT: Clinical use of polymeric scaffolds for tissue engineering often suffers from their inability to promote strong cellular interactions. Functionalization with biomolecules may improve outcomes; however, current functionalization approaches using covalent chemistry or physical adsorption can lead to loss of biomolecule bioactivity. Here, we demonstrate a novel bottom-up approach for enhancing the bioactivity of poly(L-lactic acid) electrospun scaffolds though interfacial coassembly of protein payloads with silk fibroin into nanothin coatings. In our approach, protein payloads are first added into an aqueous solution with *Bombyx mori*-derived silk fibroin. Phosphate anions are then added to trigger coassembly of the payload and silk fibroin, as well as noncovalent formation of a payload-silk fibroin coating at poly(L-lactic) acid fiber surfaces. Importantly, the coassembly process results in homogeneous distribution of protein payloads, with the loading quantity depending on payload concentration in solution and coating time. This coassembly process yields greater loading capacity than physical adsorption methods, and the payloads can be released over time in physiologically relevant conditions. We also demonstrate that the coating coassembly process can incorporate nerve growth factor and that coassembled coatings lead to significantly more neurite extension than loading via adsorption in a rat dorsal root ganglia explant culture model.

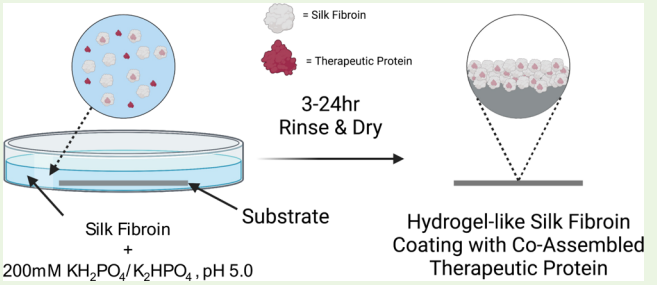

KEYWORDS: *silk fibroin, self-assembly, nerve growth factor, nerve regeneration, electrospinning*

INTRODUCTION

Electrospinning is a versatile platform for generating fibrous tissue engineering scaffolds. Compared to other nanofiber fabrication processes, that is, phase-separation and self-assembly, a variety of synthetic and natural polymers can be processed through electrospinning, and the physical characteristics of the resulting scaffold can be systematically controlled to more accurately represent the native extracellular matrix.[1,2] Biocompatible synthetic polymers, including poly(L-lactic acid) (PLLA), are routinely used in the electrospinning process as they provide high tunability and are more easily electrospun than natural polymers.[3] For example, altering the physical properties of the synthetic polymers, including molecular weight and crystallinity, allows for the generation of scaffolds with tunable mechanical properties and degradation rates.[4−6] Additionally, changes in the electrospinning environment provide systematic control over physical electrospun fiber characteristics such as diameter,[7] alignment,[8] and surface morphology.[9] This high degree of control at both the material and processing levels have led to the creation of tissue engineering scaffolds for a variety of potential medical applications including use following nerve,[10,11] cartilage,[12] and vascular[13] injury. In particular, synthetic polymers are attractive for nerve regenerative applications as they exhibit low process variability, and their high processability can be used to generate scaffolds with directional and topographical cues to direct axonal regeneration through an injury site.[11,14] Importantly, the degradation characteristics of some synthetic polymers enable appropriate mechanical robustness over the course of months, which aligns with the time frame of peripheral nerve injury repair.[14,15]

Although synthetic polymers offer many advantages, their translation into clinical practice often is impeded due to poor cell-surface interactions.[16] Thus, surface functionalization with biomolecules, often extracellular matrix proteins[17−19] or growth factors,[12,20,21] is necessary to induce cellular attachment and protein expression. Biological functionalization onto the surface of synthetic polymer surfaces is currently achieved though nonspecific adsorption[22] or chemical conjugation via biorthogonal chemistries.[23,24] Although physical adsorption can be applied to scaffolds of different chemistries and architectures, proteins are known to denature upon adsorption to surfaces, leading to a loss in biological activity.[25,26]

Received: July 29, 2023
Revised: November 8, 2023
Accepted: November 20, 2023
Published: December 18, 2023

Additionally, physical adsorption is highly dependent on the physicochemical properties of the underlying scaffold and solution environment[27] and thus often requires optimization. Alternatively, covalent conjugation can be achieved by linking specific reactive sites on the protein surface to specific chemistries within the polymer or following surface modification to the polymer surface. However, nonspecific site modifications of proteins can diminish their activity either though changes in secondary and tertiary structure or due to uncontrollable protein orientation on the substrate surface.[23] In addition, the lack of reactive groups in many biodegradable polymers limits chemical derivatization unless electrospinning is done with blends of reactive polymers, or surface pretreatments are employed, such as plasma treatment or wet chemical treatments.[28] However, these pretreatments can adversely affect scaffold biocompatibility.[29]

We have previously described a new bottom-up noncovalent approach for functionalizing electrospun scaffold surfaces based on the self-assembly of silk fibroin (SF) proteins at solid−liquid interfaces.[30,31] Our self-assembly process creates dense and adherent nanothin SF coatings by coupling surface protein adsorption with supramolecular self-assembly at the solid−liquid interface between the substrate surface and coating solution. This allows the coatings to be formed on a range of hydrophobic, hydrophilic, organic, and inorganic substrates. The amount of protein in these coatings far exceeds the quantity expected in a typical protein adsorption scenario, which generally results in saturation at submonolayer surface coverage. Unlike traditional top-down coating approaches with SF, including dip-coating or drop-casting, our self-assembled coatings do not require solvent removal though drying processes, nor do they require post-treatments to be fixed onto the surface.[32,33] Instead, our coatings continuously grow from a solid−liquid interface over time, while the substrate is immersed in the coating solution. Coating formation by SF is likely attributed to the occurrence of intra- and intermolecular interactions that promote protein−surface and protein−protein interactions upon addition of phosphate anions, with concurrent increases in β-sheet conformations during coating growth.[30,31] The nanothin nature of self-assembled SF coatings provides a strategy for modifying the chemical characteristics of a substrate surface without affecting bulk properties. Our previous studies showed that self-assembled coatings can be grown homogeneously on topologically complex PLLA electrospun scaffold surfaces without causing drastic changes to electrospun fiber diameter and alignment. Additionally, the coatings can be grown in mild aqueous buffer without any covalent conjugation chemistries or pretreatments, and they have been shown to enhance the cellular response of PLLA electrospun scaffolds using rat dorsal root ganglia explant culture models.

SF has been heavily studied as a biomaterial due to its biomedically relevant properties.[34,35] For example, SF-based materials can be generated through all-aqueous processing techniques.[36] In addition, SF exhibits exceptional biocompatibility, generally eliciting lower inflammatory responses in vivo than collagen and polylactic acid,[37,38] and its biodegradation does not generate cytotoxic byproducts.[39] Recently, a major focus of SF-based materials has been directed at its use as a drug delivery vehicle for delivery of both small and macromolecular payloads, including anticancer therapeutics[40−42] and bioactive proteins for tissue regeneration.[43−46] As a biomaterial, SF is an extremely versatile drug delivery platform for delivery of macromolecular payloads due to its ability to stabilize incorporated bioactive macromolecules in their native state.[47] This has allowed SF-based materials to be used for the delivery of sensitive growth factors to better direct cellular differentiation and proliferation.[43,48] However, when applied as coatings, either through drop-cast or dip-coating, SF is often functionalized with payloads postfabrication due to the necessity of treatments for coating fixation that can negatively affect payload bioactivity.[47]

Herein, we demonstrate that coating formation by interfacial SF assembly can provide a modular platform for creating drug-eluting surfaces to enhance the bioactivity of polymeric tissue-engineering scaffolds. We hypothesize that direct addition of biologics into the coating solution can provide a facile one-pot, noncovalent method for localizing them onto the scaffold surface though a coassembly process, which, unlike dip-coating or drop-casting, does not require postfabrication fixation steps that may disrupt payload bioactivity.[47] Additionally, we hypothesize that our process can provide more control over payload surface loading than physical adsorption without tedious optimization. To test the versatility of our approach, four model proteins varying in their size, hydrophobicity, and overall charge were tested for their ability to coassemble with SF in solution using Förster resonance energy transfer (FRET). Additionally, the effects of the coating process on the activity of the model payloads were investigated to demonstrate that the mild conditions used to generate the self-assembled coatings do not significantly reduce the activity of the payload. The ability of the model payloads to be incorporated into the nanothin SF coatings on PLLA scaffolds and the ability to tune the loading by controlling both payload concentration and coating time were assessed to investigate how payload physicochemical properties affect their ability to coassemble with the SF matrix. Payload homogeneity on PLLA electrospun scaffolds was assessed using confocal fluorescence microscopy, and the release of protein payloads under physiologically relevant conditions was investigated to demonstrate that coatings may be an effective method for delivering bioactive proteins. Finally, coassembled coatings containing nerve growth factor were generated, and the resulting cellular response from rat dorsal root ganglia was investigated using immunocytochemistry and confocal microscopy.

MATERIALS AND METHODS

All information regarding the materials, instruments, and software used in the study is included in the Supporting Information about materials section (Tables S1 and S2).

Fluorescently Labeled Proteins. Fluorophore conjugation was performed using a protocol adapted from the ThermoFisher FluoReporter FITC Protein Labeling Kit and occurred in a solution consisting of 100 mM sodium bicarbonate pH 9.0 for 1 h at room temperature. Fluorescein isothiocyanate (FITC)-tagged model proteins were purified though extensive washing with ultrapure water using 3 kDa Amicon spin filters at 4 °C. Rhodamine B isothiocyanate (RITC)-tagged SF (MW ~ 100 kDa), derived from the cocoons of *B. mori*, was purified though extensive dialysis with ultrapure water using a 3.5−5 kDa Float-A-Lyzer dialysis unit. Subsequently, the sample was lyophilized, solubilized in aqueous 6 M guanidinium thiocyanate for 90 min under gentle inversion, and dialyzed against ultrapure water using a 3.5−5 kDa Float-A-Lyzer dialysis unit to generate soluble, unassembled RITC-SF stock solutions. Fluorescently labeled payload proteins were flash frozen in single use aliquots and stored at 4 °C for no longer than 5 days after thawing before use. Care was taken to protect samples from light

https://doi.org/10.1021/acsbiomaterials.3c01042
ACS Biomater. Sci. Eng. 2024, 10, 482−496

to prevent photobleaching. Proteins generally exhibited labeling of ≤1 fluorophore per protein. Model proteins included α-lactalbumin (ALAC, accession number P00711), β-lactoglobulin (BLAC, accession number P02754), lysozyme (LYS, accession number P00698), and bovine serum albumin (BSA, accession number P02754).

Solution-Phase Förster Resonance Energy Transfer (FRET). FRET measurements were conducted to investigate the ability of model protein payloads to coassemble with the SF in solution. Briefly, fluorescently labeled proteins and commercially purchased stock solutions of degummed SF (MW ∼ 100 kDa) derived from the cocoons of *B. mori* were centrifuged at 8400 rcf for 30 min at 4 °C to remove protein aggregates immediately prior to use. Protein concentrations were quantified using a NanoDrop One Spectrometer (ThermoFisher, MA, USA) by measuring absorbance at 280 nm. We compensated for the absorbance of FITC or RITC fluorophores by measuring absorbance of our labeled proteins at 494 nm (for FITC) and 555 nm (for RITC), multiplying this absorbance by correction factors of 0.3 (for FITC) and 0.34 (for RITC) to calculate the fluorophore contribution at 280 nm and subtracting this contribution from the measured absorbance at 280 nm of the labeled protein. For SF, it was assumed that 1 abs = 1 mg/mL due to the polydispersity of the SF molecular weight from the degumming process. Extinction coefficients of 28,522, 17,600, 38,940, and 43,824 $M^{-1}cm^{-1}$ were used for ALAC, BLAC, LYS, and BSA, respectively. Solutions were prepared by consecutively adding appropriate volumes of ultrapure water, SF, fluorescently labeled proteins, and 1.25 M KH_2PO_4/K_2HPO_4 (pH 5.0) stock to generate solutions containing 0.5 mg/mL SF (molar ratio 1:3 of RITC-SF and SF), 200 mM KH_2PO_4/K_2HPO_4 pH 5.0, and the desired FITC-tagged model protein concentration. FRET emission was measured using an EnVision 2104 Multilabel Reader (PerkinElmer, MA, USA) equipped with a 485/14 nm excitation filter and 580/10 nm emission filter. In addition, FITC and RITC emissions without FRET were measured to account for fluorophore crosstalk using 485/14 nm excitation and 535/30 nm emission filters for FITC and 535/30 nm excitation and 580/10 nm emission filters for RITC in single fluorophore controls. Fluorescence measurements were measured every 1 min for 3 h. FRET emission was calculated by subtracting only FITC and RITC contributions from the total fluorescence in the FRET experiment. All measurements were measured in black 96-well plates with three biological replicates per coating solution condition (n = 3). Data represent mean ± STDEV.

Lysozyme (LYS) Solution-Phase Activity Assay. To investigate loss of payload activity due to denaturation in the coassembly coating environment, the activity of the model protein LYS in the coating solution was investigated using an EnzChek Lysozyme Assay Kit. Briefly, solutions containing between 5 and 150 μg/mL of LYS in ultrapure water or 200 mM KH_2PO_4/K_2HPO_4 pH 5.0 were prepared and incubated at 37 °C (60 rpm) with the DQ lysozyme substrate containing *Micrococcus lysodeikticus* with fluorescein-labeled cell walls. After 1 h, fluorescein fluorescence was measured using a SpectraMax M5 multimode plate reader (Molecular Devices, CA, USA) with an excitation wavelength of 494 nm and emission wavelength of 515 nm. Three biological replicates per condition were measured (n = 3), with data represented as mean ± STDEV. All measurements were conducted in black 96-well plates.

Poly(L-lactic acid) Scaffold Electrospinning. PLLA electrospun scaffolds were fabricated using the electrospinning setup previously described.[9] Briefly, PLLA dissolved in chloroform at 8 wt % was electrospun with an applied voltage of 15 keV and solution flow rate of 2 mL/h onto 15 × 15 mm glass coverslips affixed to a rotating (1000 rpm), grounded mandrel (22 cm diameter) at a collection distance of 4 cm. Scaffolds used to quantify model protein incorporation and used for confocal fluorescence imaging were spun for 15 min on bare glass coverslips, and samples used for release and DRG studies were spun for 30 min onto glass coverslips with drop-cast PLLA films (50 μL of 4 wt % PLLA in chloroform).

Fiber Characterization. Fiber diameter and alignment were quantified by using scanning electron microscopy (SEM). Fiber scaffolds were secured to a square SEM stub using a carbon tape, and then, an ∼0.5 nm layer of Au/Pd was sputter coated onto the fiber scaffolds using a Technics Hummer V Sputter Coater (Anatech USA, CA, USA). A Versa 3D Dual Beam SEM (FEI Versa, OR, USA) was used to acquire six images at 2500× magnification at different locations on the scaffold to be used for the diameter and alignment analysis. Images were acquired at a 5.0 kV accelerating voltage, 10 mm working distance, 5.0 nm spot size, and 30 μm aperture. A scaffold from n = 3 fabricated material batches was imaged for analysis. Fiber diameter was manually analyzed with ImageJ software (National Institute of Health MD, USA) by utilizing the line tool to draw a line perpendicular to the fiber orientation over the width of the fiber (excluding overlapped fibers). At least 100 fibers were analyzed per material batch.

For analyzing fiber alignment, the fast Fourier transform (FFT) function in ImageJ was used on 2500× magnification images (6 images per batch, n = 3 material batches). The oval profile plugin was used to analyze pixel intensity in radial sums in 1° increments from the FFT output image. A peak normalization method was used so that the maximum pixel intensity and corresponding angle are set to 1 and 0, respectively. Plots of the angle deviation (±50°) from the maximum intensity angle according to the normalized FFT data were generated. The area under the curve was calculated to assess the degree of fiber alignment, where the AUC can range from 1 (perfect alignment at a single angle) to 100 (no detectable alignment).

Analysis of PLLA Scaffold Surface Area. Electrospun scaffold surface area was estimated to normalize the incorporated payload mass. Briefly, PLLA fibers were removed from electrospun scaffolds and dissolved in 1 mL of dichloromethane. Absorbance measurements were conducted at 230 nm in a quartz cuvette using a NanoDrop One Spectrometer (ThermoFisher, MA, USA) and were compared to a standard curve. Fiber surface area was estimated from the calculated mass assuming that fibers were perfectly cylindrical with average diameters of 2 μm (based on analysis of scaffold SEM images), and that the density of PLLA was 1.25 g/cm^3. Results were averaged from one scaffold per batch (n = 20).

Coassembly Coating Procedure. Commercially purchased stock solutions of degummed SF (MW ∼ 100 kDa), derived from the cocoons of *B. mori*, and fluorescently labeled proteins were centrifuged at 8400 rcf for 30 min at 4 °C to remove protein aggregates immediately prior to use. Protein concentrations were measured using a NanoDrop One Spectrometer (ThermoFisher, MA, USA) by measuring absorbance at 280 nm. We compensated for the absorbance of FITC or RITC fluorophores by measuring absorbance of our labeled proteins at 494 nm (for FITC) and 555 nm (for RITC), multiplying this absorbance by correction factors of 0.3 (for FITC) and 0.34 (for RITC) to calculate the fluorophore contribution at 280 nm and subtracting this contribution from the measured absorbance at 280 nm of the labeled protein. For SF, it was assumed that 1 abs = 1 mg/mL due to the polydispersity of the SF molecular weight from the degumming process, while extinction coefficients of 28,522, 17,600, 38,940, and 43,824 $M^{-1}cm^{-1}$ were used for ALAC, BLAC, LYS, and BSA, respectively. Coassembly solutions were prepared by consecutively adding appropriate volumes of ultrapure water, SF, payload protein, and 1.25 M KH_2PO_4/K_2HPO_4 (pH 5.0) stock to generate solutions containing 0.5 mg/mL SF, 200 mM KH_2PO_4/K_2HPO_4 pH 5.0, and the desired payload protein concentration. PLLA electrospun scaffolds were immersed in freshly prepared coating solutions and allowed to coat for a set time under gentle agitation (60 rpm) at room temperature (25 °C). After coating, scaffolds were removed from the solution and were washed in 3 mL of ultrapure water for 5 min at 60 rpm. Samples were dried with a stream of air parallel to fiber alignment to mitigate fiber rearrangement. For samples prepared with fluorescently labeled SF, a molar ratio of 1:3 of RITC-SF to SF was used. Care was taken to ensure that scaffolds did not dry prior to washing and that scaffolds prepared with fluorescently labeled proteins were protected from light to minimize any photobleaching effects.

Quantification of Model Protein Incorporation. Coassembled fluorescently labeled payload incorporated into SF coatings on PLLA

https://doi.org/10.1021/acsbiomaterials.3c01042
ACS Biomater. Sci. Eng. 2024, 10, 482−496

fibers was quantified via fluorescence after dissolving the SF coatings from the PLLA substrate. Briefly, PLLA fibers from scaffolds coated with both fluorescently labeled payloads and SF (1:3 molar ratio RITC-SF:SF) using the standard coassembly procedure were cut from the underlying glass coverslip support and placed in 300 μL of 6 M guanidinium thiocyanate with constant inversion for 2 h at room temperature (25 °C). Two hundred microliters of the solution was diluted with 50 μL of ultrapure water (final guanidinium thiocyanate concentration of 4.8 M), and the fluorescence signals of the FITC-tagged proteins and RITC-tagged SF were measured using an EnVision 2104 Multilabel Reader (PerkinElmer, MA, USA) using 485/14 nm excitation and 535/30 nm emission filters for FITC and 535/30 nm excitation and 580/10 nm emission filters for RITC. All fluorescent measurements were conducted with black 96-well plates, and sample fluorescence was compared with standard curves of the fluorescently labeled proteins in 4.8 M guanidinium thiocyanate. Fibers from three independent PLLA scaffolds were used to quantify model protein incorporation (n = 3) with data representing mean ± STDEV. Crosstalk between fluorophores was accounted for in each measurement based on fluorescence of control samples only containing a single fluorophore.

Confocal Imaging of Coassembled Coatings. SF-coated scaffolds containing fluorescently labeled payload proteins and fluorescently labeled SF prepared by coating the substrate using the standard coassembly procedure were imaged using an IX-81 Confocal Microscope (Olympus NY, USA) at 20× magnification. Fluorescence images were collected using the FITC and RITC filters with an exposure time of 450 and 100 ms, respectively. Confocal samples were prepared with 100 μg/mL FITC-ALAC in the coassembly coating solution and a 1:3 molar ratio of RITC-SF to SF.

AFM Imaging of Coassembled Coatings. Dry height images of coassembled nanothin SF coatings on smooth substrates (silica wafers coated with 100 nm of TiO_2) were obtained using an MFP-3D AFM (Asylum CA, USA) operated in tapping mode. Images were collected at 1024 × 1024 pixel resolution, with a scanning speed of ∼1 Hz using aluminum reflex-coated SSS-NCHR cantilevers (NANOSENSORS Neuchâtel, Switzerland) with <2 nm tip radius, 330 kHz frequency, and a force constant of 42 N/m. Prior to coating, substrates were vigorously cleaned by sonicating for 15 min each in 10% Simple Green Original Degreaser, ultrapure water, isopropanol, acetone, and ultrapure water to remove any contamination. Samples were prepared by coating the substrate using the standard coassembly procedure, with a model protein concentration of 100 μg/mL and a coating time of 3 h. FIJI (National Institute of Health MD, USA) was used for manually determining average globule size utilizing the line tool to draw a line from edge to edge of a globule across its center. Fifty individual globules from a single image per sample were measured (n = 50) with data represented as mean ± STDEV. Coatings prepared for AFM imaging did not contain fluorescently labeled proteins.

Dynamic Light Scattering (DLS). DLS experiments were conducted at a 30 min time point on coating solutions prepared using the standard coassembly procedure, with or without model protein at a concentration of 100 μg/mL, using a Litesizer 500 (Anton Par, Graz, Austria) in quartz cuvettes using a back scattering angle of 175°. Three biological replicates per condition were tested (n = 3). Coating solutions prepared for DLS experiments did not contain fluorescently labeled proteins.

Payload Volume Contribution Calculations. Volume contributions of the model protein payloads in the SF aggregates for samples made using 100 μg/mL payload protein in coating solution was estimated utilizing the experimentally determined hydrodynamic diameters of the SF aggregates from DLS and hydrodynamic diameters of model proteins taken from the literature. Briefly, hydrated volumes of SF aggregates and model protein payloads were determined from the hydrodynamic diameters assuming perfect spheres. The total number of SF molecules contained in the SF aggregate species was assumed to be between 80 and 100 from volume analysis of individual SF globules on coated surfaces (without payloads) utilizing the particle analysis feature of the Asylum Research 16.14.216 software (Asylum CA, USA) (Figure S1). An explanation detailing the calculations for determining the number of SF molecules in the aggregated species is provided in the Supporting Information. The number of payload molecules per aggregate was calculated by multiplying this aggregation number by the experimentally determined payload:SF molar ratio, and the volume contribution of the payload molecules within an aggregate was then calculated using their hydrodynamic volumes. The theoretical total hydrodynamic diameter of the coassembled aggregate was calculated using the sum of SF aggregate and payload volume contributions, assuming a perfect sphere.

In Vitro Release of Model Payloads. PLLA scaffolds were coated for 24 h using the standard coassembly process containing 100 μg/mL FITC-tagged model payload protein and no RITC-tagged SF. The scaffolds were removed from the underlying coverslip support and incubated in 1.5 mL of 1× phosphate-buffered saline (PBS) at 37 °C with gentle shaking (60 rpm). At defined time intervals, the release media were removed and frozen at −80 °C until further analysis, and new media were added to each sample. After 14 days, the SF coatings were dissolved from the scaffolds with 6 M guanidinium thiocyanate to quantify the remaining payload not released over the 14 day study. Fluorescence measurements were conducted using an EnVision 2104 Multilabel Reader (PerkinElmer, MA, USA) equipped with 485/14 nm emission and 535/30 nm excitation filters. Sample fluorescence was compared to the standard curves for each model protein. Experiments were run in triplicate (n = 3) with data representing mean ± STDEV.

Quantification of Released LYS Activity. PLLA electrospun scaffolds were coated for 24 h in coating solutions containing 100 μg/mL of either LYS or FITC-LYS using the standard coassembly process without any RITC-SF. Coated scaffolds were peeled from the underlying coverslip support and incubated in 1.5 mL of PBS at 37 °C with gentle agitation (60 rpm). At 1 and 2 h time points, the release media were removed and immediately flash frozen and stored at −80 °C until further processing, and new media was added. LYS concentration was measured using a sandwich lysozyme enzyme-linked immunosorbent assay (ELISA) #EKN46836 according to the protocol provided by the vendor. Absorbance measurements were taken using an EnVision 2104 Multilabel Reader (PerkinElmer, MA, USA) equipped with a 450/8 nm filter. FITC-LYS concentrations were measured using an EnVision 2104 Multilabel Reader (PerkinElmer, MA, USA) equipped with 485/14 nm excitation and 535/30 nm emission filters. LYS activity was calculated by directly comparing the ELISA and fluorescence results. Three biological replicates were measured per condition (n = 3), and data is represented by mean ± STDEV.

Dorsal Root Ganglia Culture. The cellular response of SF coatings loaded with nerve growth factor (NGF, accession number: P01139) was investigated by seeding dorsal root ganglia (DRG) onto coated scaffolds and measuring the resulting neurite outgrowth. The following procedure was approved by the Rensselaer Polytechnic Institute Institutional Animal Care and Use Committee. P1 Sprague–Dawley rats (Taconic) were euthanized by rapid decapitation. Lumbar and thoracic DRG were extracted and cleaned by removing the sheath around each DRG to prevent fibroblast and other cell contamination and then collected in Ham's F-12 Nutrient Mixture on ice. Three DRG were plated on each electrospun scaffold and cultured in neurobasal medium containing B-27 supplement (2% v/v), L-glutamine (0.5 mM), and penicillin-streptomycin (1% v/v) for 4 days at 37 °C. Coassembled NGF-loaded samples were prepared using the coassembly procedure incorporating 500 ng/mL of NGF in the coassembly solution and allowing the coatings to grow for 24 h. Cellular response of the coassembled coatings was compared to scaffolds loaded with NGF via physical adsorption. Briefly, bare PLLA or 24 h SF-coated scaffolds, made using the coassembly procedure but only containing SF, were soaked in 1.5 mL 1× PBS containing 500 ng/mL NGF for 24 h, followed by a gentle wash in 3 mL of ultrapure water at 60 rpm for 5 min. All solutions were sterile filtered prior to cell work, and NGF loading via coassembly or physical adsorption occurred at room temperature. No fluorescently labeled proteins were used for the DRG studies.

https://doi.org/10.1021/acsbiomaterials.3c01042
ACS Biomater. Sci. Eng. 2024, 10, 482−496

Immunocytochemistry. Immunocytochemistry was used to assess the neurite outgrowth on the NGF-functionalized electrospun fibrous scaffolds. DRG were fixed with paraformaldehyde (4% v/v in PBS) for 15 min and then washed with PBS three times. To prevent nonspecific primary antibody binding, DRG were incubated for 1 h at room temperature in blocking solution (PBS containing BSA (5% w/v) and 0.1% v/v Triton X-100). DRG were then incubated with primary antibody RT-97 against neurofilament (1:500) in PBS containing BSA (5 wt %/v) and Tween-20 (0.1% v/v) overnight at 4 °C. DRG were then washed three times with PBS and incubated for 1 h with Alexafluor 488 donkey antimouse secondary antibody (1:1000) at room temperature. A solution of 4′,6-diamidino-2-phenylindole (DAPI) (1:1000) in PBS was then added to scaffolds and incubated for 15 min at RT protected from light to label all nuclei. Following this, DRG were washed twice with PBS and stored in PBS at 4 °C prior to imaging. Successful DRG adhesion was noted at this point, and a minimum of 12 adhered DRG were used for quantifying neurite extension/area.

DRG Confocal Microscopy. DRG on PLLA scaffolds was imaged using an IX-81 Confocal Microscope (Olympus NY, USA) and Metamorph Premier 7.7.3.0 (Molecular Devices, CA, USA) imaging software. Imaging was performed at 4× magnification with FITC and DAPI channels to acquire images of the neurofilament and nuclei, respectively. Z-series images were acquired for each field of view, and consecutive fields of view were imaged to include the entire DRG and extending neurites.

DRG Image Analysis. To analyze neurite outgrowth from the DRG, both the neurite length and area were measured. Neurite length indicates the rate of growth over the culture period, while neurite area indicates the robustness of neurite initiation. Z-series stacks in the FITC channel were first collapsed by creating the maximum intensity projection using ImageJ software (National Institute of Health MD, USA) and subtracting the background from each image (rolling = 50). All of the neurofilament images for one DRG were then stitched together using Adobe Photoshop CS2 (Adobe, CA, USA). The 10 longest neurites extending from each DRG were measured and averaged by drawing a line in ImageJ from the tip of the neurite to the edge of the DRG body. An ImageJ macro was used to assess the area of the extending neurites, excluding the DRG body. The DRG images were converted to a binary image, and then, the threshold was adjusted to include only the neurofilament signal. The oval tool was then used to exclude the DRG body, so only the area of the extending neurites was analyzed. The total pixel area was then recorded for each DRG and converted to square microns. A minimum of n = 12 DRG were imaged for each fiber group.

NGF ELISA Assay. Coassembled NGF-loaded samples were prepared using the standard coassembly process, incorporating 500 ng/mL of NGF in the coassembly solution and allowing the coatings to grow for 24 h. Physisorbed NGF-loaded samples were prepared by incubating bare PLLA scaffolds or 24 h SF-coated scaffolds, prepared using the coassembly procedure only containing SF, in 1.5 mL of 1× PBS containing 500 ng/mL NGF for 24 h followed by gentle washing with 3 mL of ultrapure water at 60 rpm for 5 min. Prepared samples were incubated in 1.5 mL of PBS at 37 °C with gentle agitation (60 rpm) for 24 h, and the release media were removed and immediately flash frozen and stored at −80 °C until further processing. NGF concentration in the samples was measured using a sandwich NGF ELISA assay #EM9RB according to the protocol provided by the vendor. Three biological replicates were measured per condition (n = 3), and data is represented by mean ± STDEV. No fluorescently labeled proteins were used for NGF ELISA assays.

Statistical Analysis. Normality of the data sets was assessed via the Shapiro−Wilk test. Both the neurite area and neurite length data were found to be normally distributed, so differences between groups were assessed with a one-way ANOVA and Tukey's post hoc test.

RESULTS AND DISCUSSION

Solution-Phase Coassembly Characterization. The ability to generate protein-loaded SF coatings for drug delivery using a one-pot bottom-up approach was investigated for controlling the bioactivity of the PLLA scaffolds. Rather than loading coatings postfabrication through physical adsorption or covalent chemical conjugation, which can lead to loss of activity of bioactive proteins,[23,27] the ability to noncovalently incorporate protein payloads directly into coatings during coating self-assembly was investigated (Scheme 1). We

Scheme 1. Schematic of the One-Pot Process for Generating Protein-Loaded Nanothin SF Coatings[a]

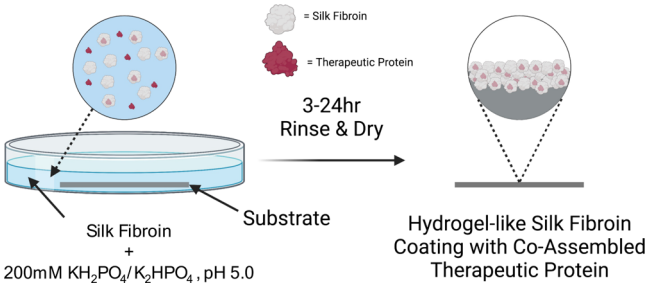

[a]Therapeutic proteins are added directly into the coating solution, where they can coassemble with the SF in solution upon addition of potassium phosphate, which facilitates SF self-assembly. The protein payloads are then incorporated into the SF coating as it forms on solid surfaces.

hypothesized that this approach could provide a modular strategy that allows for the simultaneous growth and loading of SF coatings by utilizing a phosphate-rich environment, which promotes SF self-assembly driven by β-sheet formation (Figure S2).[30,31] Additionally, we hypothesized that the conditions used to promote the assembly of the nanothin coatings (200 mM KH_2PO_4/K_2HPO_4, pH 5.0) would not drastically alter activity of the incorporated protein payloads, allowing them to be eluted from the surface in an active conformation.

Four model proteins were used to initially investigate the effects of important payload physicochemical properties, including molecular weight, charge, and hydrophobicity, on their ability to coassemble with SF into coatings (Table 1).

Table 1. Physicochemical Properties of Model Proteins Used in Study, Including Isoelectric Point (Net Charge), GRAVY Score (Hydrophobicity), and Molecular Weight (Size)[49a]

Model Protein	ALAC	BLAC	LYS	BSA
Isoelectric Point	5.0	5.1	11.4	5.8
GRAVY Score	-0.453	-0.162	-0.470	-0.475
Molecular Weight (kDa)	14.1	18.2	14.3	66.3

[a]GRAVY score was calculated from the primary sequence of proteins using the Expasy ProtParam. Pairs of model proteins used to compare each property are coded in red, blue, or green text. ALAC = β-lactalbumin, BLAC = β-lactoglobulin, LYS = lysozyme, and BSA = bovine serum albumin. Higher Gravy score indicates a more hydrophobic protein.

The four model proteins were tested included α-lactalbumin (ALAC, accession number P00711), β-lactoglobulin (BLAC, accession number P02754), lysozyme (LYS, accession number P00698), and bovine serum albumin (BSA, accession number P02754). By comparing incorporation of ALAC to BLAC, the influence of protein hydrophobicity was investigated, as the

https://doi.org/10.1021/acsbiomaterials.3c01042
ACS Biomater. Sci. Eng. 2024, 10, 482−496

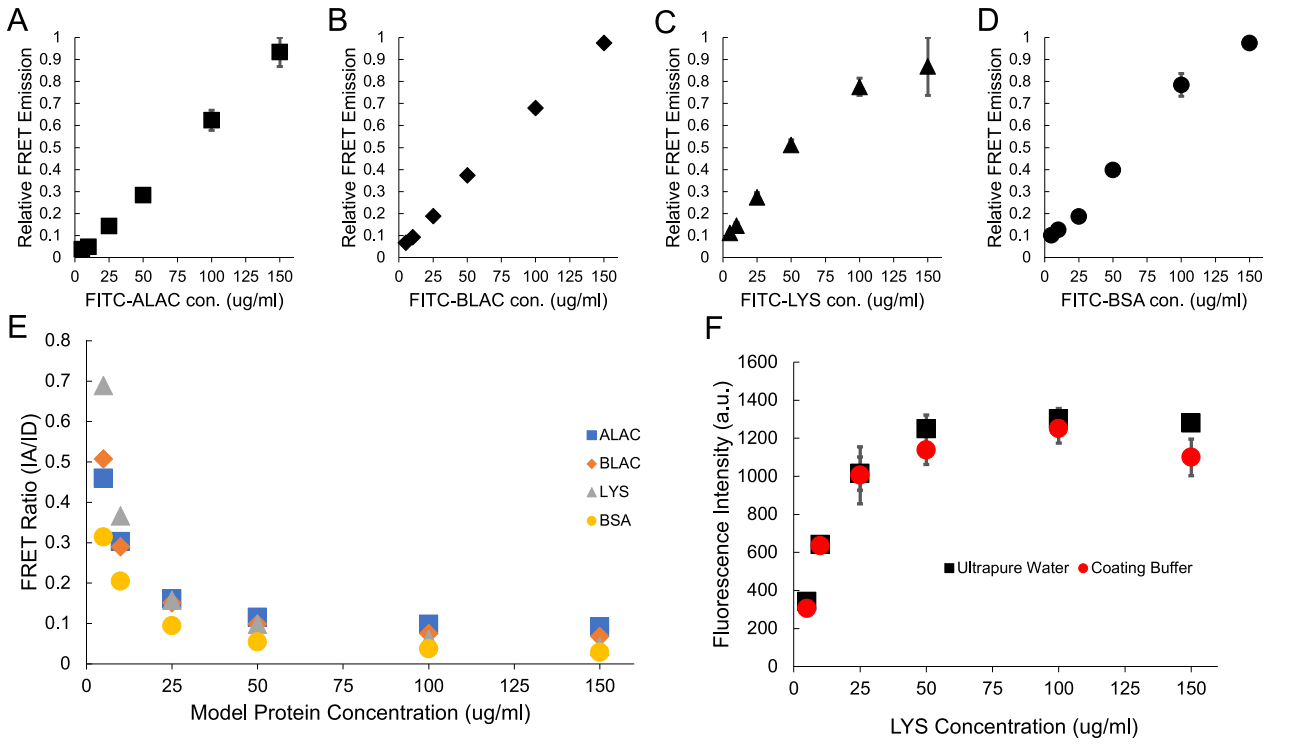

Figure 1. Solution-phase characterization of coassembly solution containing SF and model payload proteins. Relative FRET emission at the 3 h time point with varying concentration of (A) ALAC, (B) BLAC, (C) LYS, and (D) BSA in coassembly solution. The presence of FRET suggests that protein payloads are capable of coassembling with SF aggregates in the coating solution, and the degree of coassembly in the coating solution is proportional to the concentration of the protein payload. (E) Comparison of FRET ratios (acceptor emission/donor emission) for the model proteins at different concentrations in the coassembly solution. Higher FRET ratios for BLAC and LYS at lower model protein concentrations suggest coassembly of protein payloads with SF may be driven by electrostatic and hydrophobic interactions. However, at higher concentrations, these interactions may impede on payload coassembly as the SF matrix becomes more saturated with protein payload, as noted by a shift in the order of FRET ratio between the model payloads. (F) Comparison of LYS activity in coating buffer and ultrapure water monitored using an EnzChek Lysozyme Activity Kit, suggesting that the mild conditions used to generate the self-assembled SF coatings do not cause significant loss of enzymatic activity. All data is presented as mean ± STDEV, n = 3.

two proteins have substantially different GRAVY scores, −0.453 and −0.162, respectively. Additionally, by comparing the incorporation of ALAC to LYS, the influence of protein net charge was investigated as the two proteins have substantially different isoelectric points, 5.0 and 11.4, respectively. Finally, by comparing incorporation of ALAC to BSA, the influence of protein size was investigated, as the two proteins have different molecular weights, 14.1 and 66.4 kDa, respectively. For initial trials, concentrations of the model proteins in the coassembly solution ranged from 5 to 150 μg/mL, which corresponded to 1−30 wt % of model protein mass to SF mass. These concentrations were chosen because they did not cause noticeable solution-phase aggregation of the SF coating solution over a period of 24 h (data not shown).

Förester resonance energy transfer (FRET) was used to investigate the ability of the model proteins to coassemble with the SF in the 200 mM KH_2PO4/K_2HPO_4 pH 5.0 coating solution. FRET is commonly used to investigate nanoscale distances, typically 1−10 nm;[50] therefore, it was hypothesized that the presence of FRET would suggest intimate coassembly between the model proteins and SF in solution during the coating process. This was verified by the absence of FRET in a water-only no phosphate sample (data not shown), suggesting that FRET observed in the coating solution is caused by coassembly of protein payloads and SF, initiated by the addition of kosmotropic phosphate ions. For solution-phase FRET studies, the FITC/RITC donor/acceptor pair was chosen as it is a commonly used FRET pair.[51−53] Additionally, due to the low degree of fluorophore labeling, ≤ 1 fluorophore per protein, effects of the fluorophore on the coassembly is assumed to be negligible.

FRET signal was measured over an initial 3 h time period to investigate any changes in coassembly kinetics. Surprisingly, FRET emission was relatively constant over the first 3 h for each model protein at all concentrations tested (Figure S3), suggesting that coassembly of model payloads with SF occurs rapidly upon addition of KH_2PO_4/K_2HPO_4. Figure 1A−D displays the FRET emission for the model proteins at the protein concentrations tested at the final 3 h time point, relative to the FRET emission of the model protein at the highest concentration, 150 μg/mL.

Over the protein concentrations tested, the FRET signal appears to be approximately proportional to the model protein concentration in the coating environment, where an increase in model protein concentration results in an increase in observed FRET. This suggests that the amount of coassembly in the coating environment increases with the payload solution concentration. However, at even higher model protein concentrations, it would be expected that the FRET emission would no longer exhibit a monotonic relationship, which can start to be observed with LYS at the highest concentrations tested, as the SF aggregates become saturated with payload or as protein payloads begin to self-aggregate.

https://doi.org/10.1021/acsbiomaterials.3c01042
ACS Biomater. Sci. Eng. 2024, 10, 482−496

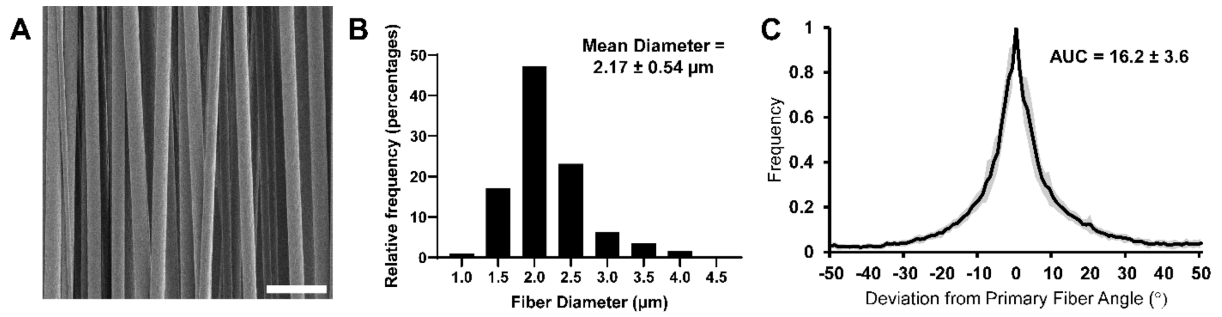

Figure 2. Electrospun fiber characterization. (A) SEM image of aligned PLLA fibers (scale bar = 10 μm). (B) Histogram of fiber diameter in μm. (C) Plot of normalized pixel intensity means from FFT images to compare fiber alignment. Shaded region around the solid line indicates ± STDEV.

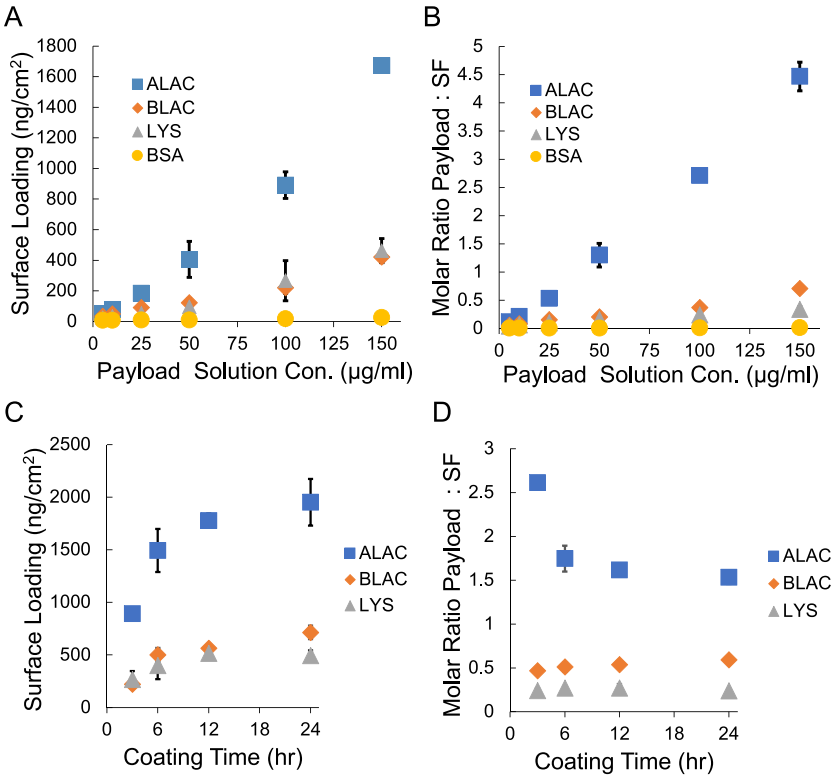

Figure 3. Surface characterization of coassembled SF coatings on PLLA electrospun scaffolds. (A) Surface loading of different model proteins with varying payload concentrations in coassembly solution. ALAC, BLAC, and LYS are capable of coassembling into coatings, showing the coassembly process is able to incorporate protein payloads with different hydrophilicities and charges. However, the size of the protein appears to affect its ability to coassemble into the nanothin SF coatings, as the mass of BSA in the coatings does not change with changing solution concentration. (B) Molar ratio of protein payload to SF in nanothin SF coatings showing that changes in surface loading are due to higher degrees of coassembly as observed in the solution-phase characterization. (C) Surface loading on PLLA electrospun scaffolds by altering the coating time, made using 100 μg/mL of model protein in the coating solution. Coassembly with protein payloads allows for continuous incorporation onto scaffold surface as coatings grow. (D) Molar ratios between model payloads and SF in the coassembled coatings. Except for ALAC, potentially due to a specific adsorption onto the PLLA surface, molar ratios of protein payloads to SF in nanothin coatings remain similar during the growth process, suggesting that the same coassembled aggregate species deposits onto the PLLA surface over time. All data is presented as mean ± STDEV, n = 3.

FRET emission between model proteins cannot be directly compared due to differences in the extents of fluorophore labeling of the model proteins. Therefore, the FRET ratio (acceptor emission/donor emission) was analyzed to normalize FRET emission to the inherent fluorescence of the donor. Here, a higher FRET ratio signifies a higher degree of solution-phase coassembly, as a higher FRET ratio denotes a higher efficiency for energy transfer between the payload donor and SF acceptor. Analysis of the FRET ratios (Figure 1E) suggests that the physicochemical properties of the model proteins affect their ability to coassemble with the SF in the coating environment. At the lowest model protein concentration of 5 μg/mL, LYS (0.727 ± 0.006) and BLAC (0.541 ± 0.021) exhibit higher FRET ratios than ALAC (0.489 ± 0.004), suggesting that solution coassembly is facilitated by electrostatic and hydrophobic attraction, which are known to increase interactions between SF-based materials and drug payloads.[54−58] However, the higher FRET ratio from LYS suggests that charge−charge interactions potentially have a larger effect on coassembly than payload hydrophobicity. The FRET ratio for BSA (0.329 ± 0.006) was lower than ALAC (0.489 ± 0.004), suggesting that the size of the protein payloads may be

https://doi.org/10.1021/acsbiomaterials.3c01042
ACS Biomater. Sci. Eng. 2024, 10, 482−496

a determining factor in terms of their ability to coassemble with SF in solution and that larger payloads may not be as readily able to coassemble with SF. Likely, as the molecular weight of the payload increases, its increase in hydrodynamic diameter causes steric hindrance between the surrounding SF molecules.

Interestingly, as the model protein concentration in the coating solution increases, there is a change in the ranking of FRET ratios between the model proteins, where ALAC begins to exhibit higher ratios compared with the other model proteins at higher payload concentrations. Although electrostatic and hydrophobic interactions facilitate coassembly of payload with SF in the coating environment, they may also hinder further coassembly as the SF aggregates become more saturated or as payload−payload interactions begin to dominate. Likely, as the payload concentration increases, electrostatic repulsion and hydrophobic interactions between payload proteins can impede the interactions between the model proteins and the SF. Interestingly, BSA exhibits the lowest FRET ratio at all concentrations tested, suggesting that the molecular weight of a payload does not have the same concentration dependence as its charge and hydrophobicity on its ability to coassemble with SF. It should be noted that the FRET ratios for all model proteins decrease as the model protein concentration in the coating solution increases, while the relative FRET signal increases. This suggests that as the payload concentration increases past ∼50 ug/mL or 10 wt/wt %, there is a larger portion of the payload that does not participate in the coassembly process. This is complemented by the observed decrease in the FRET efficiencies with increasing payload concentration, which was determined by comparing the samples to negative controls only containing the FITC-tagged model proteins without fluorescent SF (Figure S4).

The effectiveness of bioactive proteins is directly related to their ability to maintain their native structure. Therefore, any effects the coating solution environment had on the enzymatic activity of LYS were investigated using an EnzChek Lysozyme Activity Kit to ensure that the mild coating process did not adversely affect the activity of the protein payloads. LYS activity was assessed in the 200 mM KH_2PO_4/K_2HPO4 pH 5.0 coating buffer (without SF) at concentrations between 5 and 150 μg/mL and compared to its activity in ultrapure water (no potassium phosphate), (Figure 1F). Overall, there did not appear to be significant loss of LYS activity in the coating buffer compared to water, except at the highest concentration tested, which could be due to LYS self-aggregation due to kosmotropic effects of potassium phosphate. Therefore, the coassembly process could be capable of incorporating structure-sensitive protein payloads without causing significant loss of activity.

Loading of Model Payloads into Coatings. After verifying the ability of model protein payloads to coassemble with SF in the coating solution, the ability of the protein payloads to be incorporated into the nanothin SF coatings on aligned PLLA electrospun fiber scaffolds (Figure 2A) was investigated. Highly aligned rather than randomly oriented PLLA scaffolds were chosen for our studies, as they represent a "gold standard" scaffold geometry due to the ability of fiber alignment to physically regulate the elongation, orientation, and migration of neurons and other cells, which is beneficial for successful nerve tissue repair.[8,14] Additionally, alignment of fibers have been shown to enhance regeneration of axons across large 17 mm nerve gaps in vivocompared to randomly aligned fibers,[59] making them more clinically relevant. The fibers used in these studies had a diameter of 2.17 ± 0.54 μm (Figure 2B) and were highly aligned, as indicated by an AUC of 16.2 ± 3.6 after peak normalization (Figure 2C).

Surface loading curves for coatings made for 3 h on PLLA electrospun fibers containing different concentrations of model payloads in the coating solution are provided in (Figure 3A). As suggested by the solution-phase coassembly studies, the inherent physicochemical properties of the payloads greatly affect their ability to be noncovalently incorporated into the nanothin coatings via the one-pot coassembly approach. The highest model protein concentration in solution resulted in surface loadings of 1672 ± 36 ng/cm^2 (ALAC), 463 ± 72 ng/cm^2 (BLAC), 422 ± 37 ng/cm^2 (LYS), and 22 ± 6 ng/cm^2 (BSA). These masses correspond to molar ratios of model protein to SF of 4.4 ± 0.2 (ALAC), 0.71 ± 0.06 (BLAC), 0.34 ± 0.02 (LYS), and 0.015 ± 0.002 (BSA) (Figure 3B). These surface loading results correlate well with the solution-phase FRET ratios suggesting that ALAC coassembles to the highest extent followed by BLAC, LYS, and BSA at high payload concentrations. At such high payload concentrations, proteins that are smaller, more hydrophilic, and exhibit less electrostatic repulsion to the SF matrix in the coating solution can be loaded to higher extents. We hypothesize that larger payloads may create too much steric hindrance in the SF matrix and that more hydrophobic payloads may not be capable of forming favorable interactions with the SF in solution at the higher concentrations, as they may prefer to self-aggregate. Additionally, payloads that exhibit high electrostatic charge in the coating solution at higher concentrations may exhibit charge repulsion within the SF matrix, which could hinder coassembly. In general, the monotonic relationship between model protein solution concentration and resulting molar ratio for the model proteins incorporated into the coating suggests that the higher model protein loading is due to higher degree of coassembly in solution, as supported by the solution FRET assays. This is additionally shown by the relationship between model protein solution concentration and density of the payloads in the nanothin coatings (Figure S5A). Thus, the data suggests that the coassembled species in solution are directly responsible for the formation of the protein-loaded coatings at the solid interface.

Having shown the ability to generate protein-loaded SF coatings utilizing the self-assembly of SF, the ability of protein-loaded coatings to continuously grow on surfaces over time, as observed with unloaded SF-only coatings, was investigated. Substrates were exposed to coating solutions containing 100 μg/mL of each model protein for 3, 6, 12, and 24 h, and the resulting surface loaded model payload protein mass was quantified (Figure 3C). Coassembly with the model proteins in solution did not appear to inhibit the ability of the self-assembled coatings to continuously grow over a period of 24 h, although the rate of growth may be influenced by the payloads. Both of these observations are shown by comparing the change in predicted SF coating thickness calculated from the measured SF mass and PLLA surface area (Figure S6). Incorporation of ALAC, BLAC, and LYS at 24 h time points resulted in surface loadings of 1951 ± 222, 715 ± 63, and 493 ± 49 ng/cm^2, respectively, compared to 891 ± 64, 220 ± 40, and 267 ± 79 ng/cm^2 at 3 h. The ability of the self-assembled coatings to incorporate payloads as the coating grows allows the process to incorporate ∼7× more payload than loading of SF-coated

https://doi.org/10.1021/acsbiomaterials.3c01042
ACS Biomater. Sci. Eng. 2024, 10, 482−496

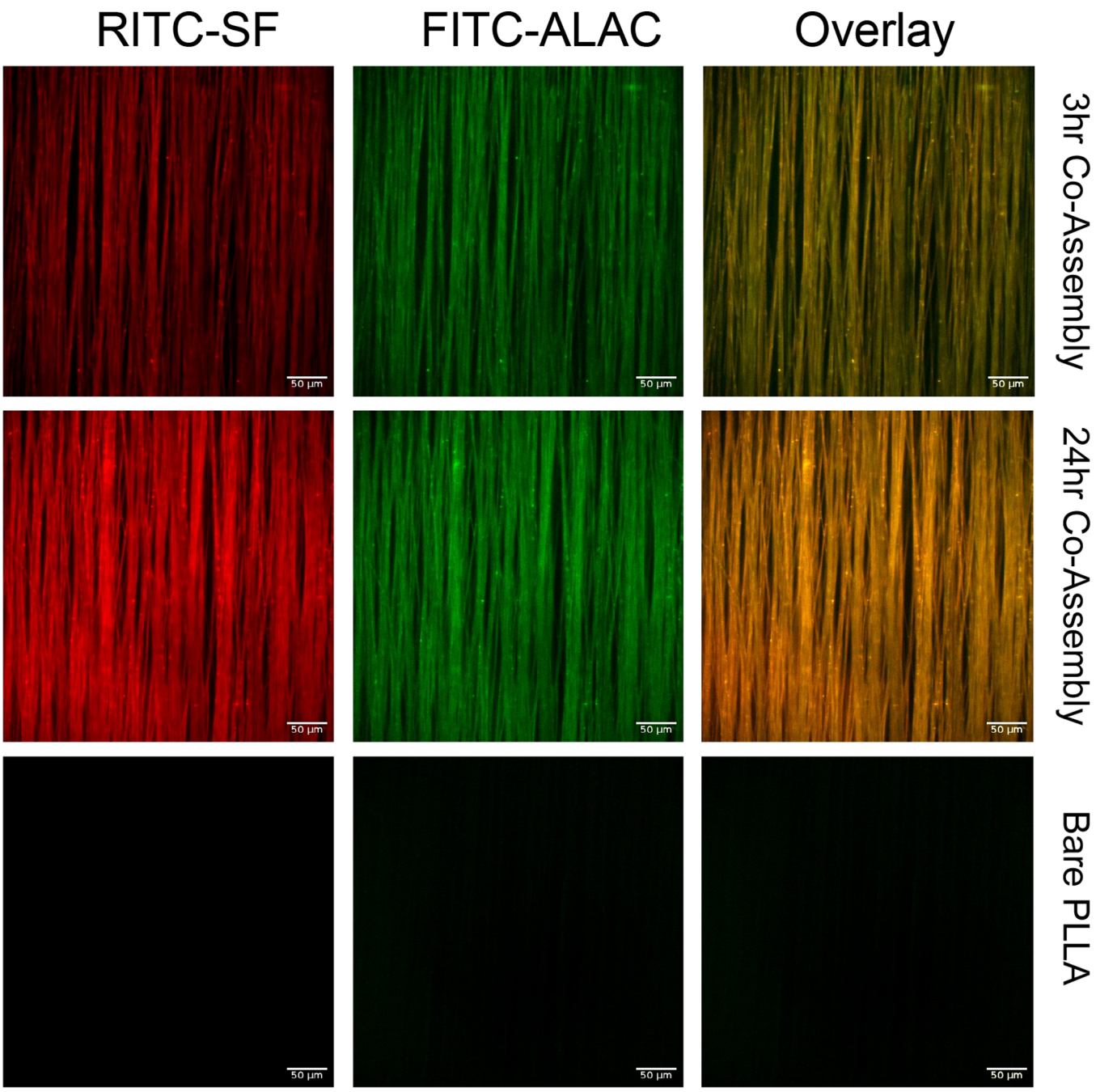

Figure 4. Confocal fluorescence images of RITC-SF and coassembled FITC-ALAC in coatings grown on PLLA electrospun scaffolds for 3 and 24 h with 100 μg/mL of FITC-ALAC in the coating solution. The uniform fluorescence in both channels suggests that the coassembled coatings are able to form evenly on the topographically complex scaffold surface, with the protein payload being homogeneously incorporated. Bare PLLA control shows that all fluorescence in both RITC and FITC channel comes from fluorescently labeled proteins and not from any background PLLA fluorescence.

scaffolds via simple physisorption (i.e., immersing a SF-coated scaffold into PBS buffer containing ALAC), which only results in 284 ± 37 ng/cm^2 loaded, although we expect that there is still some physisorption of payload proteins onto bare substrate and/or the SF coating in the coassembly case. Incorporation of BSA was not observed to increase with increasing coating times (data not shown), once again suggesting that BSA is not able to effectively coassemble with SF onto the substrate surfaces, although solution-FRET experiments suggest that a small amount of solution-phase coassembly is possible. Due to its inability to coassemble into the SF coatings, BSA was removed from the remaining portion of the study.

This increase in payload incorporation over time can be attributed to the increase in deposition of the coassembled species rather than time-dependent physical adsorption of the protein payloads onto the SF coatings, as the molar ratios between the model proteins and SF do not substantially vary over time outside of an initial coating growth stage (i.e., the first 3 h) (Figure 3D). This is additionally supported by payload densities in the nanothin coating that do not change substantially over the 24 h coating time (Figure S5B). The

https://doi.org/10.1021/acsbiomaterials.3c01042
ACS Biomater. Sci. Eng. 2024, 10, 482−496

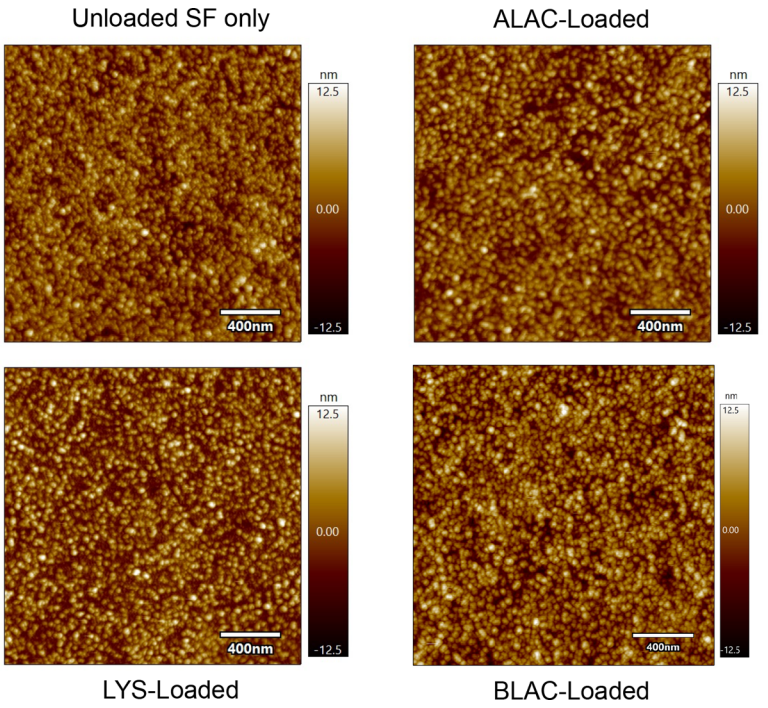

Sample	Globule Diameter (nm)
SF Only	55 ± 8
ALAC-Loaded	52 ± 9
BLAC-Loaded	58 ± 7
LYS-Loaded	52 ± 7

Figure 5. 2 μm × μm AFM height images of unloaded, ALAC-loaded, LYS-loaded, and BLAC-loaded SF coatings. Coassembly with protein payloads does not appear to drastically alter surface morphology and surface coverage compared to the unloaded control, where coatings are comprised of nanoscale globular aggregates with relatively homogeneous distributions of globule diameters.

Table 2. Hydrodynamic Diameters of the SF-Only Aggregates (Experimentally Determined), Model Protein Payloads (Taken from the Literature), Coassembled Species (Both Experimentally Determined by DLS and Theoretically Calculated Based on a Summation of SF and Payload Volumes), and Volume Contributions of Model Payloads in Coassembled Aggregates

sample	hydrodynamic diameter (nm)	experimental coassembled hydrodynamic diameter (nm)	theoretical coassembled hydrodynamic diameter (nm)	payload volume contribution (%)
SF	31 ± 2			-
ALAC[60]	3.6	32 ± 2	34.2−34.9	25−30
BLAC[61]	5.5	30 ± 3	32.6−33.0	14−17
LYS[62]	3.8	32 ± 2	31.4−31.5	3−4

only protein, which did not exhibit relatively similar molar ratios with SF over time, was ALAC. Likely, the higher ALAC:SF molar ratio at early coating time points (~2.6 at 3 h) compared to later time points (~1.5 at 24 h) can be attributed to nonspecific adsorption of free ALAC onto the PLLA surfaces at the initial stages of coating formation, which is facilitated by working near the isoelectric point of ALAC in the coating solution. Overall, these studies suggest that this coassembly approach can be a versatile method for controlling the mass of protein payloads incorporated onto a substrate surface by controlling both payload concentration in solution as well as coating time.

Distribution of Protein Payloads in Coassembled Coatings. Confocal fluorescence microscopy was used to investigate the spatial distribution of model protein payloads coassembled into SF coatings on PLLA electrospun scaffolds. Fluorescent images for both 3 and 24 h SF coatings containing RITC-tagged SF and FITC-ALAC are displayed in Figure 4. Fluorescence in the RITC channel shows that the coassembled coatings are grown on the PLLA scaffold fibers, similar to our previously reported results of self-assembled SF-only coatings.[30] The distribution of FITC-tagged ALAC in the nanothin SF coatings is also highly uniform, as observed in the FITC channel for both the 3 and 24 h samples. This suggests that the one-pot coassembly process homogeneously incorporates the payloads onto the PLLA substrate surface. However, overlay of the RITC and FITC channels at early time points does suggest some localized fluorescence, which can likely be attributed to aspecific binding of ALAC to the PLLA surface. As the coatings continuously grow over time, the payloads appear to be continuously incorporated, as indicated by the higher fluorescence intensities in the confocal images (Figure 3D). Compared to physical adsorption of ALAC onto SF self-assembled coatings in 1× PBS, (Figure S7), the incorporation of payload protein via coassembly appears to be much more homogeneously distributed.

AFM was used to investigate the surface morphology of coassembled coatings at the nanoscale on TiO_2-coated silica wafers to investigate any changes caused by coassembly with payloads (Figure 5). Images suggest that the coassembly has little effect on the assembly behavior of SF onto the substrate surface as there did not appear to be any significant changes in the surface morphology of coassembled coatings compared to SF-only coatings. All samples were composed of nanoscale globular aggregates with relatively homogeneous distributions of globule diameters, 55 ± 8 nm (unloaded SF-only), 52 ± 9 nm (ALAC loaded), 52 ± 7 nm (LYS loaded), and 58 ± 7 nm (BLAC loaded).

https://doi.org/10.1021/acsbiomaterials.3c01042
ACS Biomater. Sci. Eng. 2024, 10, 482−496

As described in the Materials and Methods section, estimated volume contributions of the model proteins in the coassembled SF globules incorporated into the coatings were calculated utilizing the hydrodynamic diameter of SF aggregates measured via DLS in the coating solution, and hydrodynamic diameters of model proteins were taken from the literature. These calculations suggest that the payload proteins account for between 3 v/v % (for LYS) to 30 v/v % (for ALAC) depending on the incorporated protein payload (Table 2). However, back calculation of the hydrodynamic diameter of the coassembled aggregates with payloads suggests that the additional volume contributed by the payload proteins does not result in a large change in the apparent hydrodynamic diameter compared to that of the SF-only species. Therefore, it is not surprising that there is no clear change in the SF globule size via AFM. This is additionally supported experimentally by measuring the coassembled species hydrodynamic diameter via DLS, which does not show a significant change in solution aggregate size. The samples of number weighted size distributions of SF-only and coassembled ALAC, BLAC, and LYS are provided in Figure S8.

Release of Coassembled Payloads. In vitro studies were conducted to investigate the release of protein payloads from the coassembled coatings. Cumulative release profiles of the model protein payloads over 14 days in 1× PBS at 37 °C are displayed in Figure 6. It is expected that the release is dominated by diffusion of the payloads out of the SF coating rather than degradation of the nanothin coatings, as there was no significant signal of RITC-SF in the release media in a SF-only sample (data not shown). The release of all protein payloads begins with an initial bolus within the first 2 days, which is consistent with diffusion-dominated release, often observed with release from hydrogels.[63−65] However, the degree of bolus release appears to be influenced by the physicochemical properties of the protein payload. ALAC exhibits the largest bolus release, with 89 ± 2% of the payload released in the first 2 days. This large bolus is likely due to the electrostatic repulsion between ALAC and SF under the release environment, as the two proteins have similar isoelectric points and therefore are expected to exhibit negative charges at pH 7.4 (isoelectric point of ALAC = 5.0, isoelectric point of SF = 4.39[66]). Over the first 2 days, LYS releases 82 ± 4%, which is slightly slower than ALAC, likely due to electrostatic attraction between positively charged LYS and negatively charged SF at pH 7.4 in PBS (isoelectric point of SF = 4.39, isoelectric point of LYS = 11.4). Of the model protein tested, BLAC has the slowest release with 69 ± 3% of the total payload released in the first 2 days. This smaller bolus is likely due to hydrophobic interactions between BLAC and SF in the coating, as BLAC is far more hydrophobic than the other model proteins even though it shares a similar isoelectric point to ALAC. Following the initial burst release, there is a steady and prolonged release for each model protein out to 14 days. Even after the 14 day release, not all the incorporated payload is released, with ∼2% of the incorporated ALAC remaining in the SF coating after release and ∼7 and ∼15% of LYS and BLAC remaining.

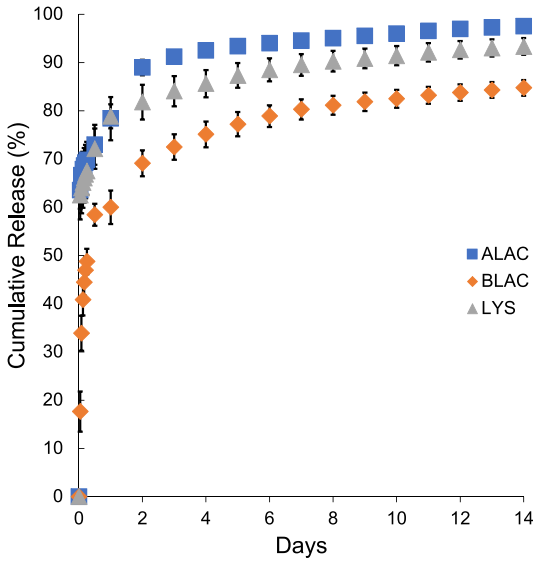

Figure 6. Cumulative release of ALAC, LYS, and BLAC into 1x PBS at 37 °C, showing that coassembled payloads can be released out to 14 days. Release profiles exhibit an initial bolus in the first 2 days, but payload still remains in the coatings even at 14 days for all model proteins. The degree of burst release is dependent on the physicochemical properties of the payloads, with more hydrophobic and more positively charged payloads releasing slower. Data is presented as mean ± STDEV, n = 3.

To assess the bioactivity of released payloads, the activity of released LYS was assessed by directly comparing the mass of FITC-LYS released measured via fluorescence, to LYS released measured using a sandwich ELISA assay. The sandwich ELISA assay relies on the use of two antibodies, which both bind to different epitopes on the target protein; therefore, it is assumed that the assayed protein is in its native and active conformation. In contrast, fluorescence measurements do not distinguish between active and inactive LYS. Therefore, assuming that the mass via fluorescence quantifies total LYS released, while mass via the ELISA assay quantifies active LYS released, the effect of incorporation into and release from the SF coating on enzymatic activity can be assessed. The release of FITC-tagged LYS from the PLLA scaffolds at 1 and 2 h time points was measured to be 536 ± 140 and 58 ± 3 ng/mL, respectively, while LYS measured using the ELISA assay was measured to be 527 ± 122 and 48 ± 5 ng/mL, respectively. Thus, it can be assumed that a majority, >80%, of the LYS released is in its active conformation. This suggests that the protein payloads incorporated into the coassembled coatings maintain bioactivity, and that the coassembled coatings can be used to release bioactive proteins in their native conformation from the surface of tissue engineering scaffolds.

NGF Coassembly and Neuron Culture. Incorporation of neurotrophic factors into synthetic nerve conduits to facilitate tissue regeneration have been of high interest.[21,46,67−69] Therefore, the ability to coassemble NGF into the nanothin SF coatings to enhance the regenerative efficacy of the PLLA electrospun scaffolds was investigated and directly compared to physical adsorption of NGF, which is a standard method for growth factor incorporation onto polymer scaffolds, by culturing primary rat DRG explants onto the coated fiber scaffolds. Although the physicochemical properties of NGF are not exactly represented by our model proteins, its hydrophobicity (GRAVY = −0.305), charge (isoelectric point = 8.82), and size (MW = 27 kDa) suggest the potential for coassembly with SF. It would be hypothesized that based on its physicochemical properties, NGF would be capable of coassembling with SF in a manner similar to LYS or BLAC and exhibit similar bolus release profiles. The DRG explant

https://doi.org/10.1021/acsbiomaterials.3c01042
ACS Biomater. Sci. Eng. 2024, 10, 482−496

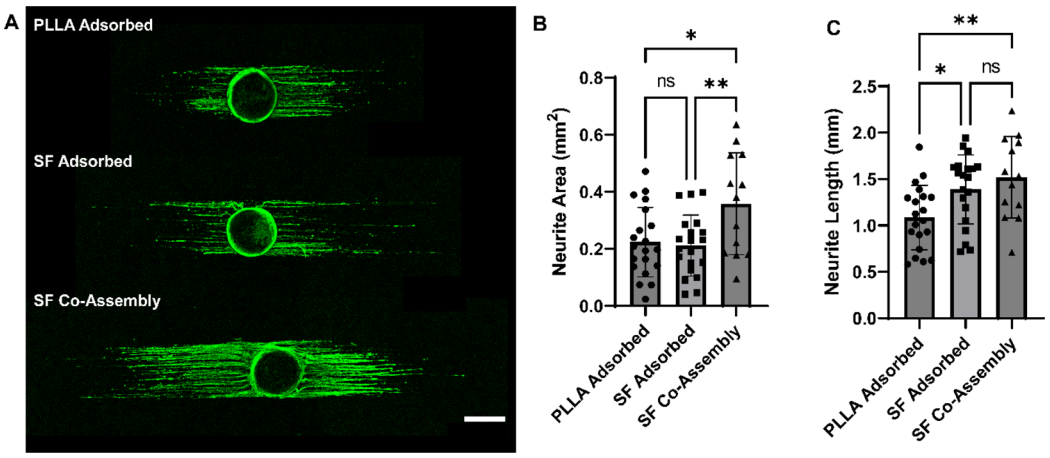

Figure 7. Coassembled SF coatings with NGF lead to a greater neurite extension density on electrospun PLLA scaffolds compared to physical adsorption of NGF onto bare PLLA and SF-coated PLLA. (A) Representative confocal microscopy images of whole DRG explants immunostained against neurofilament (green) for samples prepared by physical adsorption of NGF onto bare PLLA and SF-coated PLLA and NGF coassembled SF coated PLLA (scale bar = 500 μm). (B) Summary graph displaying total neurite area (mm^2) of DRG cultured on samples. (C) Summary graph displaying the average of the ten longest neurites (mm) for each DRG. Data are represented as mean ± STDEV. A minimum of n = 12 DRG were imaged for each fiber group. Statistical significance between scaffold groups for assays was assessed using a one-way ANOVA and Tukey's post hoc test (*p < 0.05, **p < 0.01).

model was chosen, as it is routinely used to investigate neurite outgrowth,[30,70−72] which is highly indicative of nerve regeneration.

After labeling for neurofilament using immunocytochemistry, the resulting neurite outgrowth from coassembled coatings was directly compared to bare PLLA or 24 h SF-coated scaffolds loaded with NGF via physical adsorption. Physical adsorption was used as a positive control, as is a common approach for functionalizing surfaces with growth factors,[20,22,46] and, additionally, is a common method for loading SF-based materials with biomacromolecules for drug delivery applications.[58,73,74] A 4 day DRG culture was chosen as it was assumed that the entirety of the NGF would be released according to the release studies. The resulting density of neurite outgrowth from seeded DRG, sample images for all three groups tested shown in Figure 7, was significantly enhanced with the use of the scaffolds with NGF-coassembled SF coatings compared to bare PLLA scaffolds with adsorbed NGF (*p = 0.018) and SF-coated scaffolds with adsorbed NGF(**p = 0.009), (Figure 7B). In addition to total neurite area, the 10 longest neurites from the DRG were also measured and averaged (Figure 7C), showing that both scaffolds with NGF coassembled SF coatings and scaffolds with NGF adsorbed to SF coatings had significantly longer neurite extension than the bare PLLA scaffold with adsorbed NGF. Overall, these results suggest that delivery of NGF at the scaffold surface was more effective for enhancing both the length and density of extending neurites from primary DRG explants when a coassembly process was used for loading rather than physical adsorption of NGF onto either bare PLLA or SF-coated PLLA surfaces. It should be noted that neurite outgrowth for these studies was significantly lower than the observed outgrowth from previous studies utilizing SF-coated PLLA electrospun scaffolds from Ziemba et al.[30] Those previous studies, however, were supplemented with 50 ng/mL of NGF in the neurobasal culture medium, whereas the culture media in this study was not supplemented with additional NGF so that the NGF came from surface incorporation alone.

We considered the possibility that the enhanced cellular response was due to a higher NGF surface loading via coassembly into the SF coating rather than a difference in NGF conformation (i.e., adsorbed vs coassembled). Quantification of the amount of NGF incorporated onto the scaffold surfaces was attempted by measuring the depletion of NGF from the coating solution using an NGF ELISA assay (#EM9RB). However, due to instability of the NGF in the PBS environment over the extended incubation time, this study was not possible. Therefore, we measured release of active NGF from the functionalized scaffolds into 1× PBS at 37 °C at 60 rpm to provide insight into NGF elution compared to surface-bound presentation. Over the first 24 h, the SF-coated scaffolds with adsorbed NGF released the highest amount of NGF, 4.8 ± 0.5 ng/mL, which was followed by the scaffolds where NGF was coassembled into the SF coating, 1.8 ± 0.2 ng/mL. The release from the bare PLLA coating with adsorbed NGF was undetectable by using the ELISA assay. This may be due to the low loading efficiency of NGF onto bare PLLA, resulting in NGF release below the limit of detection, as it has been previously documented that physical adsorption of growth factors onto aliphatic polyesters often results in low surface loading.[22,75] Another possibility is that NGF adsorbs strongly and denatures onto PLLA surfaces, inhibiting release of bioactive NGF. For scaffolds with SF coatings, since loading via coassembly incorporated ∼7× more model protein payload than physical adsorption with ALAC, it is counterintuitive that more NGF was released from the physisorbed sample. However, it is possible that physisorbed NGF released faster in the time frame examined, as they are distributed closer to the exterior surface compared to coassembled NGF (which should be homogeneously distributed throughout the thickness of the coating). Therefore, one possibility for the enhanced cellular response of the coassembled coatings could be due to a slower release of NGF compared to the physisorbed samples. Additionally, the coassembled coatings were shown to more homogeneously incorporate protein payloads onto the PLLA surface compared to physical adsorption, which could

https://doi.org/10.1021/acsbiomaterials.3c01042
ACS Biomater. Sci. Eng. 2024, 10, 482−496

additionally play a role in the observed enhancement of neurite area.

CONCLUSIONS

In conclusion, we have developed a versatile one-pot noncovalent method for growing nanothing coatings of SF that incorporate bioactive payloads on geometrically complex tissue engineering scaffolds. The protein-loaded coatings arise from the phosphate-induced coassembly of protein payloads with SF aggregates in solution and the continuous accumulation of the coassembled aggregates on a surface. Unlike conventional methods of functionalizing surfaces with SF and bioactive protein payloads (i.e., drop-casting, dip-coating), the mild conditions used to assemble our coatings do not cause significant loss of payload bioactivity by avoiding the use of reactive chemicals, solvent evaporation, or alcohol treatments for fixing the coatings onto the surface. As demonstrated with model proteins that vary in size, hydrophobicity, and charge, payloads with drastically different physicochemical properties can be coassembled into the nanothin coatings. However, loading is more favorable for smaller proteins. Moreover, payload incorporation is driven by hydrophobic and electrostatic attraction of SF at low payload concentrations. However, at high payload concentrations, payload−payload interactions interfere with the coassembly process, and proteins that are more hydrophilic and less charged are more favorably incorporated. Importantly, by increasing payload concentration in solution or by increasing the coating time, we can predictively increase payload loading into the nanothin coatings. Compared to physical adsorption of payloads directly onto surfaces or SF-coated surfaces, coating coassembly can yield substantially higher amounts of payload incorporation with minimal loss of payload bioactivity. Furthermore, coassembly leads to homogeneous (nonpatchy) localization of the payload onto the surfaces of electrospun fiber scaffolds, and payloads can be released from the scaffold surface over a 2 week duration, although they exhibit an initial bolus release in the first 2 days. Finally, utilizing the coassembly process to incorporate NGF onto the scaffold surface results in a better cellular response than physical adsorption onto either bare PLLA or SF-coated PLLA scaffolds. Overall, this demonstrates that coassembly of protein-loaded SF coatings can provide an enhanced strategy for controlling the surface bioactivity of synthetic electrospun scaffolds compared to conventional methods used for functionalizing scaffolds.

ASSOCIATED CONTENT

Supporting Information

The Supporting Information is available free of charge at https://pubs.acs.org/doi/10.1021/acsbiomaterials.3c01042.

Materials and equipment information; raw solution FRET data over time; FRET efficiencies; calculated model payload density; calculated SF coating thickness over time; sample confocal image of FITC-ALAC adsorption to SF; DLS of coassembly solution (PDF)

AUTHOR INFORMATION

Corresponding Author

R. Helen Zha − *Department of Chemical and Biological Engineering and Shirley Ann Jackson, Ph. D. Center for Biotechnology and Interdisciplinary Studies, Rensselaer Polytechnic Institute, Troy, New York 12180, United States;* orcid.org/0000-0002-0766-5705; Email: zhar@rpi.edu

Authors

Tanner D. Fink − *Department of Chemical and Biological Engineering and Shirley Ann Jackson, Ph. D. Center for Biotechnology and Interdisciplinary Studies, Rensselaer Polytechnic Institute, Troy, New York 12180, United States; Department of Chemistry and International Institute for Nanotechnology, Northwestern University, Evanston, Illinois 60208, United States*

Jessica L. Funnell − *Department of Biomedical Engineering, Rensselaer Polytechnic Institute, Troy, New York 12180, United States; Shirley Ann Jackson, Ph. D. Center for Biotechnology and Interdisciplinary Studies, Rensselaer Polytechnic Institute, Troy, New York 12180, United States*

Ryan J. Gilbert − *Department of Biomedical Engineering, Rensselaer Polytechnic Institute, Troy, New York 12180, United States; Shirley Ann Jackson, Ph. D. Center for Biotechnology and Interdisciplinary Studies, Rensselaer Polytechnic Institute, Troy, New York 12180, United States;* orcid.org/0000-0002-3501-6753

Complete contact information is available at: https://pubs.acs.org/10.1021/acsbiomaterials.3c01042

Author Contributions

T.D.F. and J.L.F. made equal design and experimental contributions. T.D.F. did primary planning of the study and manuscript writing with contributions from J.L.F. T.D.F. conducted all fluorophore labeling of protein stocks, FRET measurements, silk coating procedures, payload incorporation studies, release studies, AFM, and ELISA assays. J.L.F. fabricated fibers, analyzed fiber morphology characteristics, and conducted all confocal imaging, DRG experiments, and statistical analysis. R.H.Z and R.J.G. edited the manuscript.

Funding

Research reported in this publication was supported by the National Science Foundation under Award #2045510 to R.H.Z. The content does not necessarily represent the official views of the National Science Foundation. The authors additionally acknowledge the Center for Disability Services (Albany, NY) Health Innovations Incubator and Technology Center Fellowship awarded to J.L.F.

Notes

The authors declare no competing financial interest.

ABBREVIATIONS

SF, silk fibroin; $CHCl_3$, chloroform; DMSO, dimethyl sulfoxide; DRG, dorsal root ganglia; NGF, nerve growth factor; FITC, fluorescein isothiocyanate; RITC, rhodamine b isothiocyanate; PBS, phosphate-buffered saline; PLLA, poly-L-lactic acid; SEM, scanning electron microscopy; AFM, atomic force microscopy

REFERENCES

(1) Xue, J.; Wu, T.; Dai, Y.; Xia, Y. Electrospinning and Electrospun Nanofibers: Methods, Materials, and Applications. *Chem. Rev.* **2019**, *119*, 5298−5415.

(2) Wang, X.; Ding, B.; Li, B. Biomimetic electrospun nanofibrous structures for tissue engineering. *Mater. Today* **2013**, *16*, 229−241.

(3) Nemati, S.; Kim, S. J.; Shin, Y. M.; Shin, H. Current progress in application of polymeric nanofibers to tissue engineering. *Nano Convergence* **2019**, *6*, 36.

(4) von Recum, H. A.; Cleek, R. L.; Eskin, S. G.; Mikos, A. G. Degradation of polydispersed poly(l-lactic acid) to modulate lactic acid release. *Biomaterials* **1995**, *16*, 441−447.
(5) Zhang, X.; Nakagawa, R.; Chan, K. H. K.; Kotaki, M. Mechanical Property Enhancement of Polylactide Nanofibers through Optimization of Molecular Weight, Electrospinning Conditions, and Stereocomplexation. *Macromolecules* **2012**, *45*, 5494−5500.
(6) Shasteen, C.; Choy, Y. B. Controlling degradation rate of poly(lactic acid) for its biomedical applications. *Biomed Eng. Lett.* **2011**, *1*, 163.
(7) Tan, S.-H.; Inai, R.; Kotaki, M.; Ramakrishna, S. Systematic parameter study for ultra-fine fiber fabrication via electrospinning process. *Polymer* **2005**, *46*, 6128−6134.
(8) Wang, H. B.; Mullins, M. E.; Cregg, J. M.; Hurtado, A.; Oudega, M.; Trombley, M. T.; Gilbert, R. J. Creation of highly aligned electrospun poly-L-lactic acid fibers for nerve regeneration applications. *J. Neural Eng.* **2009**, *6*, No. 016001.
(9) D'Amato, A. R.; Puhl, D. L.; Ziemba, A. M.; Johnson, C. D. L.; Doedee, J.; Bao, J.; Gilbert, R. J. Exploring the effects of electrospun fiber surface nanotopography on neurite outgrowth and branching in neuron cultures. *PLoS One* **2019**, *14*, No. e0211731.
(10) Yang, F.; Murugan, R.; Ramakrishna, S.; Wang, X.; Ma, Y.-X.; Wang, S. Fabrication of nano-structured porous PLLA scaffold intended for nerve tissue engineering. *Biomaterials* **2004**, *25*, 1891−1900.
(11) Zhang, X.; Qu, W.; Li, D.; Shi, K.; Li, R.; Han, Y.; Jin, E.; Ding, J.; Chen, X. Functional Polymer-Based Nerve Guide Conduits to Promote Peripheral Nerve Regeneration. *Adv. Mater. Interfaces* **2020**, *7*, 2000225.
(12) Ma, Z.; Gao, C.; Gong, Y.; Shen, J. Cartilage tissue engineering PLLA scaffold with surface immobilized collagen and basic fibroblast growth factor. *Biomaterials* **2005**, *26*, 1253−1259.
(13) Hu, J.; Sun, X.; Ma, H.; Xie, C.; Chen, Y. E.; Ma, P. X. Porous nanofibrous PLLA scaffolds for vascular tissue engineering. *Biomaterials* **2010**, *31*, 7971−7977.
(14) Li, Y.; Dong, T.; Li, Z.; Ni, S.; Zhou, F.; Alimi, O. A.; Chen, S.; Duan, B.; Kuss, M.; Wu, S. Review of advances in electrospinning-based strategies for spinal cord regeneration. *Mater. Today Chem.* **2022**, *24*, No. 100944.
(15) Schaub, N. J.; Johnson, C. D.; Cooper, B.; Gilbert, R. J. Electrospun Fibers for Spinal Cord Injury Research and Regeneration. *J. Neurotraum* **2016**, *33*, 1405−1415.
(16) Capuana, E.; Lopresti, F.; Ceraulo, M.; Carrubba, V. L. Poly-l-Lactic Acid (PLLA)-Based Biomaterials for Regenerative Medicine: A Review on Processing and Applications. *Polymers* **2022**, *14*, 1153.
(17) Sousa, M. C. A. de; Rodrigues, C. A. V.; Ferreira, I. A. F.; Diogo, M. M.; Linhardt, R. J.; Cabral, J. M. S.; Ferreira, F. C. Functionalization of Electrospun Nanofibers and Fiber Alignment Enhance Neural Stem Cell Proliferation and Neuronal Differentiation. *Front. Bioeng. Biotechnol.* **2020**, *8*, No. 580135.
(18) He, L.; Tang, S.; Prabhakaran, M. P.; Liao, S.; Tian, L.; Zhang, Y.; Xue, W.; Ramakrishna, S. Surface Modification of PLLA Nanoscaffolds with Laminin Multilayer by LbL Assembly for Enhancing Neurite Outgrowth. *Macromol. Biosci* **2013**, *13*, 1601−1609.
(19) Truong, Y. B.; Glattauer, V.; Briggs, K. L.; Zappe, S.; Ramshaw, J. A. M. Collagen-based layer-by-layer coating on electrospun polymer scaffolds. *Biomaterials* **2012**, *33*, 9198−9204.
(20) Xia, B.; Lv, Y. Dual-delivery of VEGF and NGF by emulsion electrospun nanofibrous scaffold for peripheral nerve regeneration. *Mater. Sci. Eng., C* **2018**, *82*, 253−264.
(21) Tang, S.; Zhu, J.; Xu, Y.; Xiang, A. P.; Jiang, M. H.; Quan, D. The effects of gradients of nerve growth factor immobilized PCLA scaffolds on neurite outgrowth in vitro and peripheral nerve regeneration in rats. *Biomaterials* **2013**, *34*, 7086−7096.
(22) Shen, H.; Hu, X. Growth factor loading on aliphatic polyester scaffolds. *Rsc Adv.* **2021**, *11*, 6735−6747.
(23) Wong, L. S.; Khan, F.; Micklefield, J. Selective Covalent Protein Immobilization: Strategies and Applications. *Chem. Rev.* **2009**, *109*, 4025−4053.
(24) Meldal, M.; Schoffelen, S. Recent advances in covalent, site-specific protein immobilization. *F1000research* **2016**, *5*, 2303 DOI: 10.12688/f1000research.9002.1.
(25) Zoungrana, T.; Findenegg, G. H.; Norde, W. Structure, Stability, and Activity of Adsorbed Enzymes. *J. Colloid Interface Sci.* **1997**, *190*, 437−448.
(26) Vertegel, A. A.; Siegel, R. W.; Dordick, J. S. Silica Nanoparticle Size Influences the Structure and Enzymatic Activity of Adsorbed Lysozyme. *Langmuir* **2004**, *20*, 6800−6807.
(27) Rabe, M.; Verdes, D.; Seeger, S. Understanding protein adsorption phenomena at solid surfaces. *Adv. Colloid Interfac* **2011**, *162*, 87−106.
(28) Taskin, M. B.; Ahmad, T.; Wistlich, L.; Meinel, L.; Schmitz, M.; Rossi, A.; Groll, J. Bioactive Electrospun Fibers: Fabrication Strategies and a Critical Review of Surface-Sensitive Characterization and Quantification. *Chem. Rev.* **2021**, *121*, 11194−11237.
(29) Sánchez, L. D.; Brack, N.; Postma, A.; Pigram, P. J.; Meagher, L. Surface modification of electrospun fibres for biomedical applications: A focus on radical polymerization methods. *Biomaterials* **2016**, *106*, 24−45.
(30) Ziemba, A. M.; Fink, T. D.; Crochiere, M. C.; Puhl, D. L.; Sapkota, S.; Gilbert, R. J.; Zha, R. H. Coating Topologically Complex Electrospun Fibers with Nanothin Silk Fibroin Enhances Neurite Outgrowth in Vitro. *Acs Biomater Sci. Eng.* **2020**, *6*, 1321−1332.
(31) Zha, R. H.; Delparastan, P.; Fink, T. D.; Bauer, J.; Scheibel, T.; Messersmith, P. B. Universal nanothin silk coatings via controlled spidroin self-assembly. *Biomater Sci-uk* **2019**, *7*, 683−695.
(32) Wang, X.; Kim, H. J.; Xu, P.; Matsumoto, A.; Kaplan, D. L. Biomaterial Coatings by Stepwise Deposition of Silk Fibroin. *Langmuir* **2005**, *21*, 11335−11341.
(33) Servoli, E.; Maniglio, D.; Motta, A.; Predazzer, R.; Migliaresi, C. Surface Properties of Silk Fibroin Films and Their Interaction with Fibroblasts. *Macromol. Biosci* **2005**, *5*, 1175−1183.
(34) Altman, G. H.; Diaz, F.; Jakuba, C.; Calabro, T.; Horan, R. L.; Chen, J.; Lu, H.; Richmond, J.; Kaplan, D. L. Silk-based biomaterials. *Biomaterials* **2003**, *24*, 401−416.
(35) Vepari, C.; Kaplan, D. L. Silk as a biomaterial. *Prog. Polym. Sci.* **2007**, *32*, 991−1007.
(36) Rockwood, D. N.; Preda, R. C.; Yucel, T.; Wang, X.; Lovett, M. L.; Kaplan, D. L. Materials fabrication from Bombyx mori silk fibroin. *Nat. Protoc* **2011**, *6*, 1612−1631.
(37) Thurber, A. E.; Omenetto, F. G.; Kaplan, D. L. In vivo bioresponses to silk proteins. *Biomaterials* **2015**, *71*, 145−157.
(38) Meinel, L.; Hofmann, S.; Karageorgiou, V.; Kirker-Head, C.; McCool, J.; Gronowicz, G.; Zichner, L.; Langer, R.; Vunjak-Novakovic, G.; Kaplan, D. L. The inflammatory responses to silk films in vitro and in vivo. *Biomaterials* **2005**, *26*, 147−155.
(39) Kundu, B.; Rajkhowa, R.; Kundu, S. C.; Wang, X. Silk fibroin biomaterials for tissue regenerations. *Adv. Drug Deliver Rev.* **2013**, *65*, 457−70.
(40) Gou, S.; Xie, D.; Ma, Y.; Huang, Y.; Dai, F.; Wang, C.; Xiao, B. Injectable, Thixotropic, and Multiresponsive Silk Fibroin Hydrogel for Localized and Synergistic Tumor Therapy. *Acs Biomater Sci. Eng.* **2020**, *6*, 1052−1063.
(41) Subia, B.; Dey, T.; Sharma, S.; Kundu, S. C. Target Specific Delivery of Anticancer Drug in Silk Fibroin Based 3D Distribution Model of Bone−Breast Cancer Cells. *Acs Appl. Mater. Inter* **2015**, *7*, 2269−2279.
(42) Xie, M.; Fan, D.; Chen, Y.; Zhao, Z.; He, X.; Li, G.; Chen, A.; Wu, X.; Li, J.; Li, Z.; Hunt, J. A.; Li, Y.; Lan, P. An implantable and controlled drug-release silk fibroin nanofibrous matrix to advance the treatment of solid tumour cancers. *Biomaterials* **2016**, *103*, 33−43.
(43) UEBERSAX, L.; MATTOTTI, M.; PAPALOIZOS, M.; MERKLE, H.; GANDER, B.; Meinel, L. Silk fibroin matrices for the controlled release of nerve growth factor (NGF). *Biomaterials* **2007**, *28*, 4449−4460.
(44) Baker, L. A.; Xu, L.; Akher, F. B.; Robertson, M. K.; Pugsley-DeBruyn, L.; Ma, C. X.; Liu, X.; Frampton, J. P.; Rainey, J. K. Nerve Growth Factor-Binding Engineered Silk Films Promote Neuronal

Attachment and Neurite Outgrowth. *Adv. Funct. Mater.* **2022**, *32*, 2205178.
(45) Zhang, W.; Zhu, C.; Ye, D.; Xu, L.; Zhang, X.; Wu, Q.; Zhang, X.; Kaplan, D. L.; Jiang, X. Porous Silk Scaffolds for Delivery of Growth Factors and Stem Cells to Enhance Bone Regeneration. *PLoS One* **2014**, *9*, No. e102371.
(46) Carvalho, C. R.; Chang, W.; Silva-Correia, J.; Reis, R. L.; Oliveira, J. M.; Kohn, J. Engineering Silk Fibroin-Based Nerve Conduit with Neurotrophic Factors for Proximal Protection after Peripheral Nerve Injury. *Adv. Healthcare Mater.* **2021**, *10*, 2000753.
(47) Lu, S.; Wang, X.; Lu, Q.; Hu, X.; Uppal, N.; Omenetto, F. G.; Kaplan, D. L. Stabilization of Enzymes in Silk Films. *Biomacromolecules* **2009**, *10*, 1032−1042.
(48) Ding, Z.; Fan, Z.; Huang, X.; Lu, Q.; Xu, W.; Kaplan, D. L. Silk−Hydroxyapatite Nanoscale Scaffolds with Programmable Growth Factor Delivery for Bone Repair. *Acs Appl. Mater. Inter* **2016**, *8*, 24463−24470.
(49) Woo, J.; Parimal, S.; Brown, M. R.; Heden, R.; Cramer, S. M. The effect of geometrical presentation of multimodal cation-exchange ligands on selective recognition of hydrophobic regions on protein surfaces. *J. Chromatogr A* **2015**, *1412*, 33−42.
(50) Algar, W. R.; Hildebrandt, N.; Vogel, S. S.; Medintz, I. L. FRET as a biomolecular research tool — understanding its potential while avoiding pitfalls. *Nat. Methods* **2019**, *16*, 815−829.
(51) Li, L.; Zhang, Q.; Chen, B.; Guo, M.; Yang, Q.; Zhang, Y.; Zhang, M. Nano-Bio Interface-Guided Nanoparticle Protein Corona Antigen for Immunoassays and Immunoimaging in a Complex Matrix. *ACS Appl. Bio Mater.* **2022**, *5*, 841−852.
(52) Schrimpf, W.; Jiang, J.; Ji, Z.; Hirschle, P.; Lamb, D. C.; Yaghi, O. M.; Wuttke, S. Chemical diversity in a metal−organic framework revealed by fluorescence lifetime imaging. *Nat. Commun.* **2018**, *9*, 1647.
(53) Zou, J.-J.; Wei, G.; Xiong, C.; Yu, Y.; Li, S.; Hu, L.; Ma, S.; Tian, J. Efficient oral insulin delivery enabled by transferrin-coated acid-resistant metal-organic framework nanoparticles. *Sci. Adv.* **2022**, *8*, No. eabm4677.
(54) Hines, D. J.; Kaplan, D. L. Mechanisms of Controlled Release from Silk Fibroin Films. *Biomacromolecules* **2011**, *12*, 804−812.
(55) Lammel, A.; Schwab, M.; Hofer, M.; Winter, G.; Scheibel, T. Recombinant spider silk particles as drug delivery vehicles. *Biomaterials* **2011**, *32*, 2233−2240.
(56) Lammel, A. S.; Hu, X.; Park, S.-H.; Kaplan, D. L.; Scheibel, T. R. Controlling silk fibroin particle features for drug delivery. *Biomaterials* **2010**, *31*, 4583−4591.
(57) Numata, K.; Kaplan, D. L. Silk-based delivery systems of bioactive molecules. *Adv. Drug Deliver Rev.* **2010**, *62*, 1497−1508.
(58) Yucel, T.; Lovett, M. L.; Kaplan, D. L. Silk-based biomaterials for sustained drug delivery. *J. Controlled Release* **2014**, *190*, 381−397.
(59) Kim, Y.; Haftel, V. K.; Kumar, S.; Bellamkonda, R. V. The role of aligned polymer fiber-based constructs in the bridging of long peripheral nerve gaps. *Biomaterials* **2008**, *29*, 3117−3127.
(60) Spöttel, J.; Brockelt, J.; Falke, S.; Rohn, S. Characterization of Conjugates between α-Lactalbumin and Benzyl Isothiocyanate—Effects on Molecular Structure and Proteolytic Stability. *Molecules* **2021**, *26*, 6247.
(61) Elofsson, U. M.; Dejmek, P.; Paulsson, M. A. Heat-induced aggregation of β-lactoglobulin studied by dynamic light scattering. *Int. Dairy J.* **1996**, *6*, 343−357.
(62) Parmar, A. S.; Muschol, M. Hydration and Hydrodynamic Interactions of Lysozyme: Effects of Chaotropic versus Kosmotropic Ions. *Biophys. J.* **2009**, *97*, 590−598.
(63) Chen, Y.; Guo, X.; Mensah, A.; Wang, Q.; Wei, Q. Nature-Inspired Hydrogel Network for Efficient Tissue-Specific Underwater Adhesive. *ACS Appl. Mater. Interfaces* **2021**, *13*, 59761 DOI: 10.1021/acsami.1c20548.
(64) Kumari, S.; Bargel, H.; Anby, M. U.; Lafargue, D.; Scheibel, T. Recombinant Spider Silk Hydrogels for Sustained Release of Biologicals. *ACS Biomater. Sci. Eng.* **2018**, *4*, 1750 DOI: 10.1021/acsbiomaterials.8b00382.
(65) Ding, Z.; Zhou, M.; Zhou, Z.; Zhang, W.; Jiang, X.; Lu, X.; Zuo, B.; Lu, Q.; Kaplan, D. L. Injectable Silk Nanofiber Hydrogels for Sustained Release of Small-Molecule Drugs and Vascularization. *Acs Biomater Sci. Eng.* **2019**, *5*, 4077−4088.
(66) Leal-Egaña, A.; Scheibel, T. Interactions of cells with silk surfaces. *J. Mater. Chem.* **2012**, *22*, 14330−14336.
(67) Zhu, L.; Jia, S.; Liu, T.; Yan, L.; Huang, D.; Wang, Z.; Chen, S.; Zhang, Z.; Zeng, W.; Zhang, Y.; Yang, H.; Hao, D. Aligned PCL Fiber Conduits Immobilized with Nerve Growth Factor Gradients Enhance and Direct Sciatic Nerve Regeneration. *Adv. Funct. Mater.* **2020**, *30*, 2002610.
(68) Zhou, G.; Chang, W.; Zhou, X.; Chen, Y.; Dai, F.; Anwar, A.; Yu, X. Nanofibrous Nerve Conduits with Nerve Growth Factors and Bone Marrow Stromal Cells Pre-Cultured in Bioreactors for Peripheral Nerve Regeneration. *Acs Appl. Mater. Inter* **2020**, *12*, 16168−16177.
(69) Lee, H. S.; Jeon, E. Y.; Nam, J. J.; Park, J. H.; Choi, I. C.; Kim, S. H.; Chung, J. J.; Lee, K.; Park, J. W.; Jung, Y. Development of a regenerative porous PLCL nerve guidance conduit with swellable hydrogel-based microgrooved surface pattern via 3D printing. *Acta Biomater* **2022**, *141*, 219−232.
(70) Au, N. P. B.; Kumar, G.; Asthana, P.; Gao, F.; Kawaguchi, R.; Chang, R. C. C.; So, K. F.; Hu, Y.; Geschwind, D. H.; Coppola, G.; Ma, C. H. E. Clinically relevant small-molecule promotes nerve repair and visual function recovery. *NPJ Regen. Med.* **2022**, *7*, 50.
(71) Taylor, C. S.; Behbehani, M.; Glen, A.; Basnett, P.; Gregory, D. A.; Lukasiewicz, B. B.; Nigmatullin, R.; Claeyssens, F.; Roy, I.; Haycock, J. W. Aligned Polyhydroxyalkanoate Blend Electrospun Fibers as Intraluminal Guidance Scaffolds for Peripheral Nerve Repair. *ACS Biomater. Sci. Eng.* **2023**, *9*, 1472−1485.
(72) Puhl, D. L.; Funnell, J. L.; Fink, T. D.; Swaminathan, A.; Oudega, M.; Zha, R. H.; Gilbert, R. J. Electrospun fiber-mediated delivery of neurotrophin-3 mRNA for neural tissue engineering applications. *Acta Biomater.* **2022**, *155*, 370 DOI: 10.1016/j.actbio.2022.11.025.
(73) Wang, X.; Hu, X.; Daley, A.; Rabotyagova, O.; Cebe, P.; Kaplan, D. L. Nanolayer biomaterial coatings of silk fibroin for controlled release. *J. Controlled Release* **2007**, *121*, 190−199.
(74) Choi, M.; Choi, D.; Hong, J. Multilayered controlled drug release silk fibroin nano-film by manipulating secondary structure. *Biomacromolecules* **2018**, *19*, 3096−3103.
(75) Shen, H.; Hu, X.; Bei, J.; Wang, S. The immobilization of basic fibroblast growth factor on plasma-treated poly(lactide-co-glycolide). *Biomaterials* **2008**, *29*, 2388−2399.